Supplementary Information for

Antidark Soliton Complexes in a Fiber Laser

Xiao Hu,[1,2,†] Jun Guo,[3,†] Guangwei Hu,[2] Seongwoo Yoo,[2] Dingyuan Tang[1*]

[1]*Future Technology School, Shenzhen Technology University, Shenzhen 518118, China*
[2]*School of Electrical and Electronic Engineering, Nanyang Technological University, Nanyang Avenue, Singapore 639798, Singapore*
[3]*Jiangsu Key Laboratory of Laser Materials and Devices, School of Physics and Electronic Engineering, Jiangsu Normal University, Xuzhou, China*

This Supplementary Information consists of the following sections:

Section 1: Theoretical derivation on energy-width scaling of antidark solitons.

Theoretically, the light propagation in single mode fibers in the near-zero GVD regime is described by the normalized NLSE of the form in the normal dispersion regime [Phys. Lett. A **395**, 127226 (2021)]:

$$i\frac{\partial u}{\partial z}-\frac{1}{2}\frac{\partial^2 u}{\partial \tau^2}+|u|^2=i\frac{\beta_3}{6}\frac{\partial^3 u}{\partial \tau^3} \tag{1.1}$$

Where $\beta_3$is the normalized third-order dispersion (TOD) coefficient of the single mode fiber. Under small amplitude approximation, E. q (1.1) has the solution of,

$$u(z,\tau)=[u_0+a(z,\tau)]\exp[iu_0{}^2z+i\phi(z,\tau)] \tag{1.2}$$

Where a is a small amplitude, and has the form of,

$$a(z,\tau)=-u_0\frac{\mu^2(\gamma+4\sigma)}{2(\gamma+\sigma)}\operatorname{sech}^2 Z \tag{1.3}$$

Where u_0 is the amplitude of the continuous wave background, and $\mu=\varepsilon/u_0$, ε is an arbitrary value, $\sigma=\pm1$, $\gamma=1/\beta_3u_0$, $Z\approx\mu u_0(\tau-u_0\sigma z)$ and,

$$\phi(Z)=[\sigma\mu(\gamma+4\sigma)/(\gamma+\sigma)]\tanh Z+\phi_0 \tag{1.4}$$

Where ϕ_0 is an arbitrary phase factor. Mathematically, E. q (1.1) admits not only antidark soliton solution but also conventional bright soliton solutions in the anomalous dispersion regime, in the form of $\operatorname{sech}(\tau)$. Based on E. q (1.3), we first plot the energy-width relation of the antidark solitons and compare the energy-width relation with the conventional bright solitons, the results is shown in Fig. S1. It is obvious that compared to the conventional bright solitons, antidark solitons present advantageous in energy-pulse scaling, that is, at same pulse width, the energy of antidark soliton scales like $E\propto sech^4(\tau)$, while for bright solitons, it scales like $E\propto sech^2(\tau)$. Thus, these results could open a way for the generation of high-

energy, ultrashort pulses that arise from self-phase modulation and higher-order cavity dispersion.

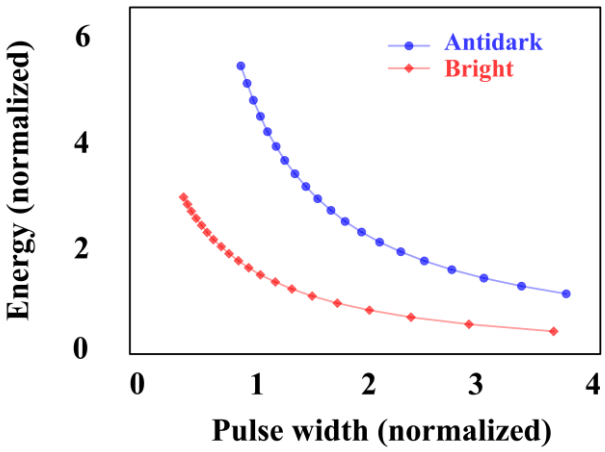

Fig. S1 Energy-width relationship for antidark and conventional bright solitons. Blue dotted line: energy-pulse width relation of antidark solitons; The energy is calculated based on E. q (1.3), e.g, $E_{antidark} = a^2 \propto sech^4(\tau)$; Red square line: energy-pulse width relation of conventional solitons, e.g, $E_{bright} = sech^2(\tau)$. Parameters used in the theoretical model: $\beta_3 = 0.5$; $u_0 = 1$; $\sigma = -1$; $\mu = 1.5$.

In addition to the energy-width scaling plot, we also theoretically investigate the influence of TOD on the energy-width scaling, a typical result is presented in Fig. S2. Briefly, we have shown that the merit of energy-width scaling of antidark solitons could further be stressed by increasing the strength of TOD. It is clear that as the TOD coefficient is increased from 0.4 to 0.6, the energy of the antidark solitons undergoes significant amplification.

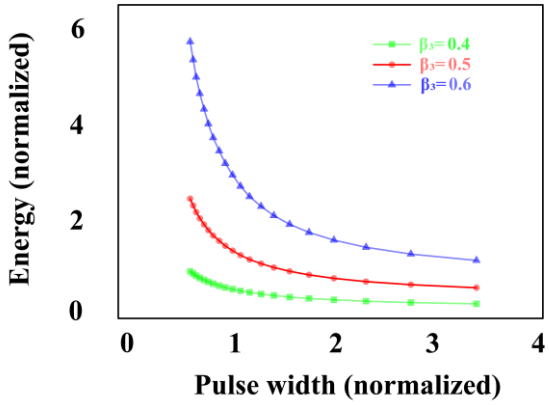

Fig. S2 Energy-width relationship for antidark under different strengths of TOD. Blue triangular line: $\beta_3 = 0.6$; Red dotted line: $\beta_3 = 0.5$; Green dotted line: $\beta_3 = 0.4$.

Section 2: Experimental setup and results

Section 2.1: Experimental setup

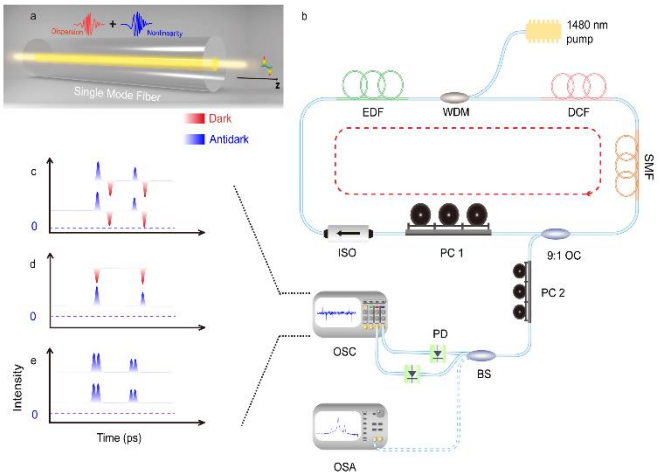

Fig. S3 A schematic of the fiber ring laser. Orange circle line: Single mode fiber; Green circle line: Erbium-doped fiber; Red circle line: Dispersion compensation fiber. Erbium-doped fiber (OFS-EDF80 with GVD coefficient of $\beta_2 = 63.4\ ps^2\ km^{-1}$), dispersion shifted fiber (DCF with GVD coefficient of $\beta_2 = 5.1\ ps^2\ km^{-1}$) and stand single mode fiber (SMF-28 with GVD coefficient of $\beta_2 = -23.8\ ps^2\ km^{-1}$).

Fig. S3 shows a schematic of our fiber ring laser. Experimentally, to separately observe the two orthogonal polarization components of the light field, the laser output is first sent to a fiber pigtailed polarization beam splitter and then monitored with a high-speed detection system consisting of two 40GHz photodetectors (Newport, Model 1014) and a 33GHz bandwidth real-time oscilloscope (Agilent Technologies, DSA-93204 A). An extra polarization controller (PC2) is inserted between the laser output and the beam splitter to balance the linear polarization change induced by the lead fibers. Finally, an optical spectrum analyzer (Yokogawa, AQ6375) is used to monitor the optical spectrum of the laser emission.

Section 2.2: Estimation of ZGVD point in the experimental setup

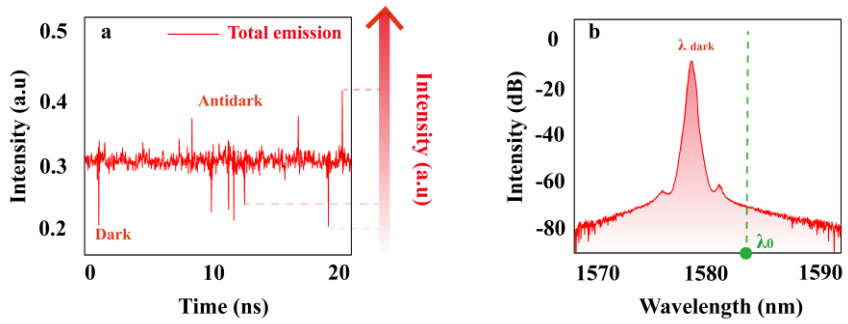

Fig. S4 Coexistence of dark and antidark solitons in normal GVD close to the ZGVD point. a. Temporal trace. **b.** Optical spectra of a.

In our experimental studies, the central wavelength of the ZGVD point is estimated through an "spectral analysis method". We first operate the fiber laser at near zero dispersion regime by selecting 3 m EDF, 8 m SMF, and 0.1 m DCF, thus the net averaged cavity dispersion is tuned at near ZGVD regime, i.e, ($\beta_{2,ave} = 0.005\, ps^2/km$). Experimentally, the central wavelength of laser emissions could be slightly tuned (e.g, from 1580 to 1588 nm in our experimental setup). In prior studies, we have shown that at near ZGVD regime, independent formation of scalar dark and scalar bright solitons is possible. To verify this result, in the current experimental setup, we first operate the laser at the net normal cavity dispersion regime by tuning the central wavelength of emission to the shorter wavelength side, i.e, 1582nm, a state of coexistence of scalar dark and antidark solitons is obtained as shown in Fig. S4. Theoretical studies have shown that antidark solitons are only supported by third-order dispersion [Phys. Rev. A **44**, R1446(R) (1991)], in this context, the appearance of antidark solitons in Fig. S4(a) indicates that the net cavity dispersion is now tuned very close to the ZGVD point. In parallel with the dark soliton formations, when we shift the central wavelength of laser emission to the longer wavelength, i.e, 1585nm, a typical scalar bright soliton emission state is obtained. In particular, in such an active fiber laser (without mode-locking mechanism), the formation of

bright solitons is associated with several modulation instabilities [J. Opt. Soc. Am. B **31**, 3050-3056 (2014)], under this formation mechanism, the bright solitons always characterized by a quantization feature as shown in Fig. S5. Starting from such a pure bright soliton emission state, if we continue vary the intracavity PC paddles until the central wavelength of the laser emission shift towards to 1583nm, a state of coexistence of scalar bright and dark solitons is obtained as shown in Fig. S6. Upon formation, the scalar dark and bright solitons could either independently propagate across the ZGVD point or undergo attractive interactions, leading to the formation of ordinary dark-bright solitons (ODBSs) [8]. Moreover, if we compare the spectral characteristics shown in Figs. S4(b) and S5(c) to those shown in S6(c), it is obvious that the optical spectrum shown in Fig. S6(c) is a result of the super-position of two parts, the shaded part is due to the scalar dark solitons, and the blue shaded part belongs to the bright solitons. We emphasize that this coexistence state is only possible at the near ZGVD point in a laser, where the spectra of solitons have well extended across the ZGVD point. Indeed, with the aid of such a "spectral analysis" technique, we can thus estimate that the ZGVD point of our experimental setup is roughly around 1583 nm.

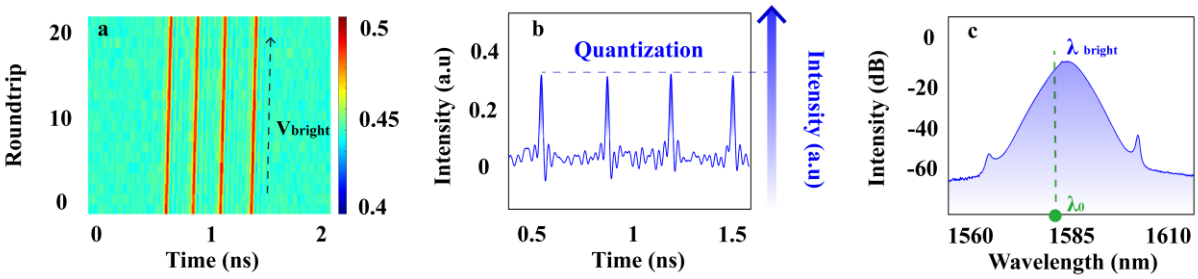

Fig. S5 Formation of bright solitons in the anomalous GVD regime. a. Evolution of bright solitons over 20 cavity roundtrips. **b.** Temporal trace on scalar bright solitons. **c.** Optical spectrum of a.

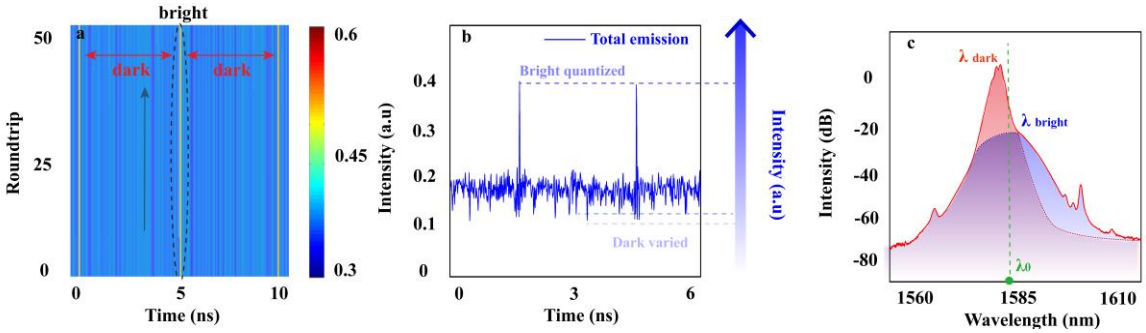

Fig. S6 Coexistence of scalar dark and bright solitons across the ZGVD point. a. Evolution of bright and dark solitons over 50 cavity roundtrips. **b.** Temporal trace on scalar dark and bright solitons. **c.** Optical spectra of a.

Section 2.3: Experimental results on scalar dark and antidark solitons

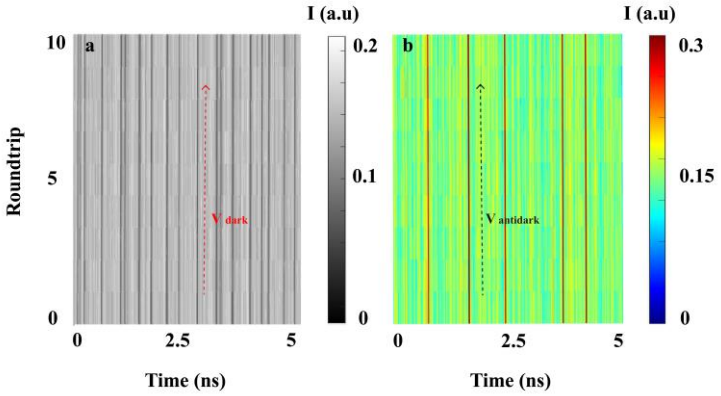

Fig. S7 Evolution of the dark and antidark solitons. a. Evolution of dark solitons over ten cavity roundtrips. **b.** Evolution of antidark solitons over ten cavity roundtrips.

The main purpose of the paper is to experimentally investigate the various third-order dispersion supported soliton molecules (CDSMs), including vector dark-anitdark solitons, vector antidark solitons, and vector antidark soliton molecules, formed in a weakly birefringent fiber laser at near zero-group velocity dispersion (ZGVD) points. However, in a weakly birefringent fiber cavity because the XPM effect will greatly complicate the soliton dynamics, in order to easily understand the formed vector soliton dynamics, we first built a scalar fiber laser cavity (follow the same cavity structure as reported in [Phys. Lett. A **395**, 127226 (2021)]) to study intrinsic properties of the scalar dark and antidark solitons. Specifically, we have

repeated the formation of dark and antidark solitons and confirmed that the formation of antidark solitons is a general feature of light propagation in SMFs under dominate effect of TOD. Unlike the formation of dark solitons which is threshold-less [Opt. Express. **22**, 19831 (2014)], the appearance of antidark solitons would require slightly large intracavity power. Fig. S4 shows the typical evolution states we measured on the emission of pure dark and antidark solitons respectively. In [Phys. Lett. A **395**, 127226 (2021)], we have theoretically studied the properties of dark and antidark solitons and showed that due to the anti-phase properties, the dark and antidark solitons always propagate at opposite directions in the cavity undergoing repulsive interactions, this feature is clearly unfolded in Fig. S7, for instance, the dark solitons are travelling towards right (marked by the red arrow pointing direction) while the antidark solitons are travelling towards left (marked by the black arrow pointing direction). In addition, the moving speed of the dark and antidark solitons is remarkably slower than that of the conventional bright solitons formed in the mode-locked laser systems [Laser & Photonics Reviews. **12**, 1800009 (2018)].

Section 2.4: Quantify of normalized TOD coefficient

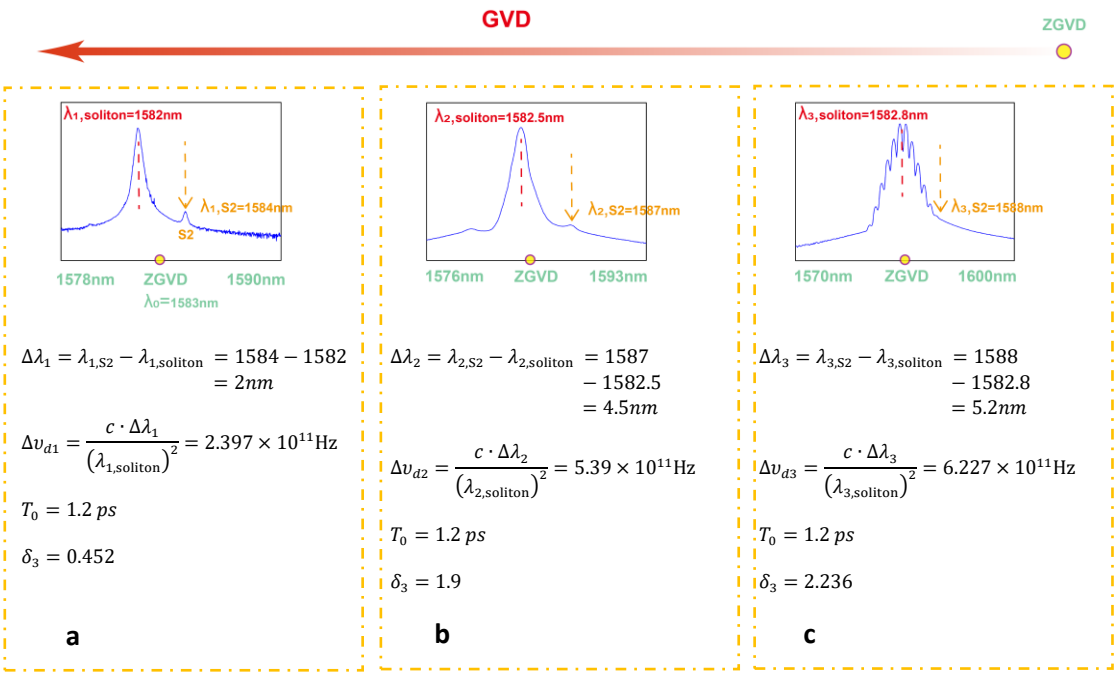

$\Delta\lambda_1 = \lambda_{1,S2} - \lambda_{1,\text{soliton}} = 1584 - 1582 = 2nm$

$\Delta\upsilon_{d1} = \frac{c \cdot \Delta\lambda_1}{(\lambda_{1,\text{soliton}})^2} = 2.397 \times 10^{11}\text{Hz}$

$T_0 = 1.2\ ps$

$\delta_3 = 0.452$

a

$\Delta\lambda_2 = \lambda_{2,S2} - \lambda_{2,\text{soliton}} = 1587 - 1582.5 = 4.5nm$

$\Delta\upsilon_{d2} = \frac{c \cdot \Delta\lambda_2}{(\lambda_{2,\text{soliton}})^2} = 5.39 \times 10^{11}\text{Hz}$

$T_0 = 1.2\ ps$

$\delta_3 = 1.9$

b

$\Delta\lambda_3 = \lambda_{3,S2} - \lambda_{3,\text{soliton}} = 1588 - 1582.8 = 5.2nm$

$\Delta\upsilon_{d3} = \frac{c \cdot \Delta\lambda_3}{(\lambda_{3,\text{soliton}})^2} = 6.227 \times 10^{11}\text{Hz}$

$T_0 = 1.2\ ps$

$\delta_3 = 2.236$

c

Fig. S8 Quantify of TOD in the laser system. Calculated normalized TOD coefficients, from left to right a-c, for the pure dark soliton, antidark soliton and antidark soliton molecule emission states based on the frequency shift of the soliton sidebands.

In Supplementary section 2.2, we have conducted a series of experiments to estimate that the central wavelength of our laser system is located at 1583nm. Furthermore, in order to confirm that the antidark solitons are formed as a result of TOD, we introduce a spectral analysis method to quantify the normalized TOD in our experiments. It is to note that in general case, a dispersive wave cannot be phase matched with a fundamental soliton whose wave number lies in a range of forbidden for a linear dispersive wave. However, the presence of TOD can lead a phase-matched situation in which energy is transferred from soliton to the dispersive wave at a specific frequency [Phys. Rev. A **79,** 023824 (2009)], and this frequency is given by a relatively simple expression,

$$\Delta\nu_d T_0 \approx \frac{(1+4{\delta_3}^2)}{4\pi\delta_3} \tag{2.1}$$

Where $\Delta\nu_d = \nu_d - \nu_s$, and ν_s and ν_d are the carrier frequencies associated with the soliton and the dispersive wave, respectively. In our experiment, fine tuning the intracavity PC paddles will shift the central wavelength of the laser emissions (from Fig. S8a to S8c, the central wavelength of laser emission is approaching the ZGVD point), meanwhile, associated with the central wavelength shift, the enhancement of TOD will also perturb the dispersive waves emitted by solitons, as a result, the frequency shift of spectral sidebands become obvious. In particular, by using the spectral analysis method introduced in the supplementary section 2.2, we first can approximate the ZGVD wavelength of our laser locates at 1583nm. Therefore, starting from the vector dark soliton emission state ($\lambda_{1,\mathrm{soliton}} = 1582nm$), if we shift our central wavelength of laser emission to $\lambda_{3,\mathrm{soliton}} = 1582.8nm$, we could expect that the TOD effect will be enhanced, to support this claim, we have calculated the normalized TOD coefficient based on E.q. (2.1). In our experiment, from the autocorrelation trace which we appended in Figure 8b, if a sech-form pulse shape is assumed, the pulse width of the antidark soliton is around 1.2ps, therefore, in our calculation, we use $T_0 = 1.2\,ps$. Then from the sideband frequency shift

caused by the enhancement of TOD effect, through relationship (2.1) we can estimate the normalized TOD coefficient in our experiment to be $\delta_3 = 0.452, 1.9,\ 2.236$ for the cases of pure dark soliton emission state, antidark soliton emission state, and antidark soliton molecule emission state, respectively. The calculation results indicate that as we shift the central wavelength of the laser emission towards the ZGVD point, the TOD effect becomes more and more obvious.

Section 3: The simulation model

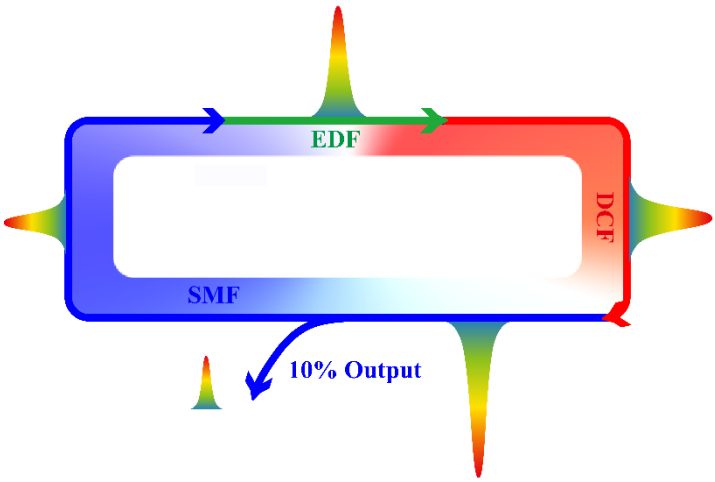

Fig. S9 Schematic configuration of the fiber laser cavity used for numerical simulations. Blue solid line: Single mode fiber; Green solid line: Erbium-doped fiber; Red solid line: Dispersion compensation fiber. The color gradient indicates the evolution of the effective cavity dispersion. Blue color: anomalous cavity dispersion; Red color: normal cavity dispersion.

To make the simulation results directly comparable with the experimental observations, our simulations were conducted based on the real experimental fiber laser configuration as shown in Fig. S3. Fig. S9 shows the schematic configuration of the fiber laser cavity used for numerical simulations. We adopt a technique known as "pulse tracing" to simulate the laser operation. Briefly, when a light pulse circulates inside the cavity, the local fiber group velocity dispersion and birefringence varies with the fibers used. At different positions of the cavity, the pulse may present slightly different pulse shapes and energies. We note that as our cavity length is much shorter than the pulse dispersion and nonlinearity length, the dispersion-managed features are not dominant. Numerically, we have output the light pulse at different positions of the ring cavity and verified that the pulse properties are mainly determined by the averaged cavity parameters rather than that of the single segment of the fiber ring laser [Phys. Rev. Lett. **82**, 3988 (1999)].

The light propagation in the fibers is described by the coupled extended Ginzburg-Landau equations (CGLEs) [Appl. Phys. Rev. **6**, 021313 (2019)],

$$\begin{aligned}\frac{\partial u}{\partial z} &= +\delta\frac{\partial u}{\partial t} - \frac{i\beta_{2u}}{2}\frac{\partial^2 u}{\partial t^2} + \frac{\beta_{3u}}{6}\frac{\partial^3 u}{\partial t^3} + i\gamma(|u|^2 + \frac{2}{3}|v|^2)u + \frac{g}{2}u + \frac{g}{2\Omega_g{}^2}\frac{\partial^2 u}{\partial t^2} \\ \frac{\partial v}{\partial z} &= -\delta\frac{\partial v}{\partial t} - \frac{i\beta_{2v}}{2}\frac{\partial^2 v}{\partial t^2} + \frac{\beta_{3v}}{6}\frac{\partial^3 v}{\partial t^3} + i\gamma(|v|^2 + \frac{2}{3}|u|^2)v + \frac{g}{2}v + \frac{g}{2\Omega_g{}^2}\frac{\partial^2 v}{\partial t^2}\end{aligned} \tag{3.1}$$

Where u and v are the normalized envelopes of the optical fields at different wavelengths. $\delta = \frac{1}{2}(\frac{1}{v_{gv}} - \frac{1}{v_{gu}})$ is the inverse group velocity difference between the modes. β_{2u} and β_{2v} are the second-order dispersion coefficients, β_{3u} and $\beta_{3\mathrm{v}}$ are the third-order dispersion (TOD) coefficients for the lights. γ represents the averaged nonlinear coefficient of the fiber, g is the saturable gain coefficient of the gain fiber and Ω_g is the gain bandwidth. For the light propagation in the undoped fibers, $g = 0$. In our simulations, the gain saturation is described by,

$$\mathrm{g}=\mathrm{g}_0 \exp[-\frac{\int(|u|^2+|v|^2)dt}{E_{sat}}] \tag{3.2}$$

Where $g_0$is the small signal gain coefficient and E_{sat} is the saturation energy. When the light meets the cavity output port, 10% of the light intensity is deducted from the light fields, and the rest of the light is then reinjected into the cavity as the input for the next round of cavity circulation. We used the standard split-step method to solve the coupled extended CGLEs (3.1). The numerical calculations were made on a $400\ ps$ window and the periodic boundary condition was used. Numerically, we studied the coexistence of vector dark and vector antidark solitons and the formation of vector dark-antidark solitons based on E. q. (3.1). In addition, we also simulated the interactions between the scalar antidark solitons polarized along the same polarization axis by setting the XPM coupling coefficient to 2,

$$\begin{aligned}\frac{\partial u}{\partial z} &= +\delta\frac{\partial u}{\partial t} - \frac{i\beta_{2u}}{2}\frac{\partial^2 u}{\partial t^2} + \frac{\beta_{3u}}{6}\frac{\partial^3 u}{\partial t^3} + i\gamma(|u|^2 + 2|v|^2)u + \frac{g}{2}u + \frac{g}{2\Omega_g{}^2}\frac{\partial^2 u}{\partial t^2} \\ \frac{\partial v}{\partial z} &= -\delta\frac{\partial v}{\partial t} - \frac{i\beta_{2v}}{2}\frac{\partial^2 v}{\partial t^2} + \frac{\beta_{3v}}{6}\frac{\partial^3 v}{\partial t^3} + i\gamma(|v|^2 + 2|u|^2)v + \frac{g}{2}v + \frac{g}{2\Omega_g{}^2}\frac{\partial^2 v}{\partial t^2}\end{aligned} \tag{3.3}$$

Noteworthy mentioning that although our current simulations are based on the CGLEs, under appropriate conditions, for example, if the gain bandwidth is larger than the soliton spectral bandwidth and the laser gain is balanced by the cavity losses, the CGLEs could be

mathematically reduced to CNLSE [*Optical Solitons: From Fibers to Photonic Crystals* (Academic Press, 2003)].

Section 4: Simulation results on formation of vector antidark and vector dark solitons

Fig. S10 shows the initial conditions we used for the simulations on antidark solitons. The details on the simulation parameters on Fig. S11 are described in Tab. S1.

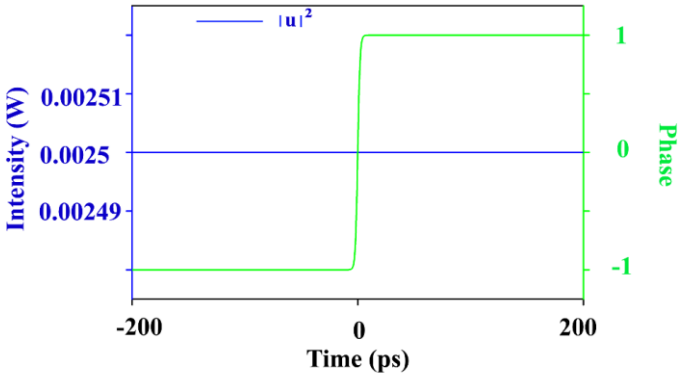

Fig. S10 Initially injected CW beam with a small phase jump embedded. Bule solid line: intensity of CW beam. Green solid line: embedded phase jump at the middle position of the CW beam.

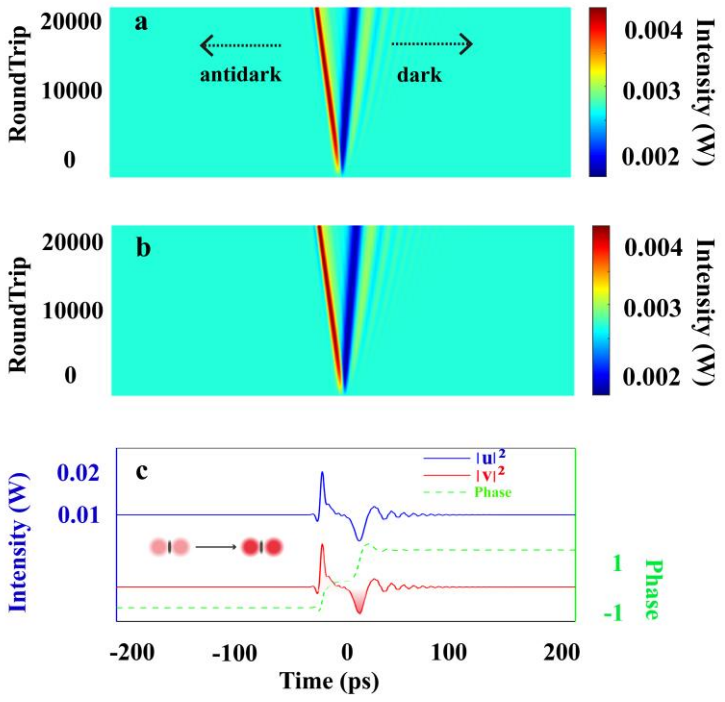

Fig. S11 Simulation results on coexistence of vector dark and antidark solitons. a Evolution of antidark and dark soliton along the horizontal polarization axis. **b** Evolution of antidark and dark soliton along the vertical polarization axis. **c** Blue/red solid line: antidark and dark soliton formed along horizontal/vertical polarization axes at the last cavity round trip. Green solid line: associated phase jump with the dark and antidark soliton.

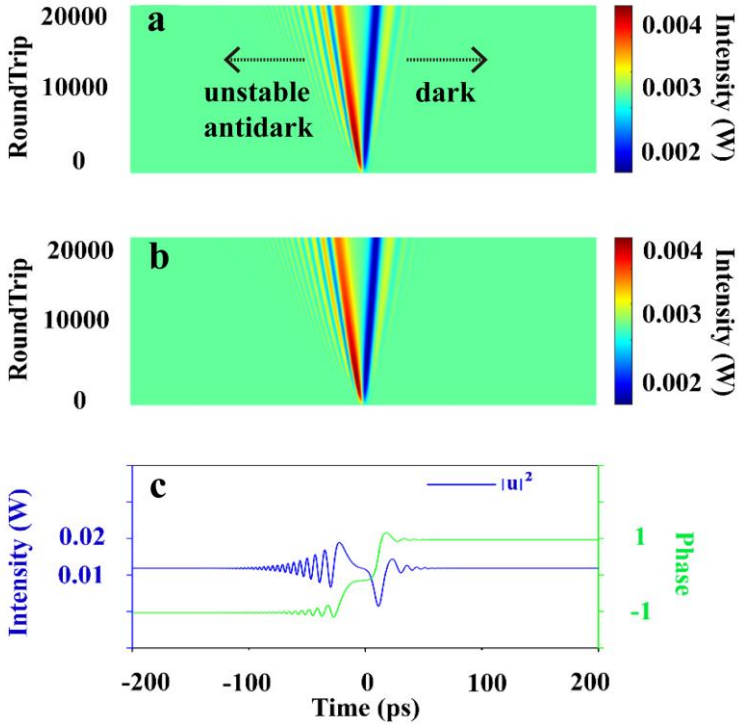

Fig. S12 Unstable formation of vector antidark solitons. **a** Evolution of antidark and dark soliton along the horizontal polarization axis. **b** Evolution of antidark and dark soliton along the vertical polarization axis. **c** Blue solid line: antidark and dark soliton at the last cavity round trip. Green solid line: associated phase jump with the dark and antidark soliton.

We start the simulation with two arbitrary weak CW beams and on top of the CW beams, a small phase jump is embedded, a typical pulse shape is presented in Fig. S10. We let the light circulate in the ring cavity. Our simulation is based on E. q. (3.1). To propagate the light in net normal GVD regime, we set the GVD coefficients of SMF along orthogonally polarized directions to be $\beta_{2u} = \beta_{2v} = -22.93\, ps^2/km$ (See Supplementary Tab. S1). We deliberately increase the coefficient of TOD to $0.1\, ps^3/km$ which can be experimentally realized by tuning the PC paddles until the central wavelengths of laser emissions locate even closer to ZGVD point, under appropriate power level, the dark and antidark solitons of

comparable pulse widths are always simultaneously formed and they travel to the opposite directions in the cavity as displayed in Fig. S11. Numerically we found that the antidark solitons can only be formed when effect of TOD dominates the second order cavity dispersion. If we decrease the TOD coefficient to $\beta_{3u} = \beta_{3u} = 0.01 ps^3/km$, no stable antidark solitons could be formed as shown in Supplementary Fig. S12. In comparison with the formation of scalar antidark solitons, numerically it was found that with the aid of cross-phase coupling (XPC), the power threshold for creating such a vector antidark soliton emission state is lower, suggesting that the XPC may provide a strong attractive force between them [Nonlinear Dyn. **94**, 1351 (2018)].

Initial Pulse Shape	Averaged cavity parameters	SMF	EDF	DCF
$u = v$ $= A \cdot \exp(i \cdot tanh(Bt))$ $A = 0.05;$ $B = 1;$	*Net averaged cavity dispersion:* $\beta_{2u,ave} = \beta_{2v,ave} =$ 0.01 ps^2/km $\beta_{3u,ave} = \beta_{3v,ave} =$ 0.1 ps^3/km *Net averaged cavity birefringence:* $\delta_{ave} = 0.0005\ ps/km$ γ =0.003 $(Wm)^{-1}$ Cavity loss: 10%	$\beta_{2,u}$= $\beta_{2,v}$= -22.93 ps^2/km $L_B = 5\ km$ L=8.0 m	$\beta_{2,u}$= $\beta_{2,v}$= 63.4 ps^2/km g_0 = 90 km^{-1} Ω_g= 80 nm E_s=0.001 nJ $L_B = 0.5\ km$ L=3 m	$\beta_{2,u}$= $\beta_{2,v}$= 5.1 ps^2/km $L_B = 0.5\ km$ L= 0.2 m

Tab. S1. Parameters used for obtaining Fig. S11.

Section 5: Simulation results on formation of vector dark-antidark solitons

Fig. S13 shows the initial pulse shape we used for the simulations on vector dark-antidark solitons. The details of the simulation parameters for Fig. S14 are described in Tab. S2.

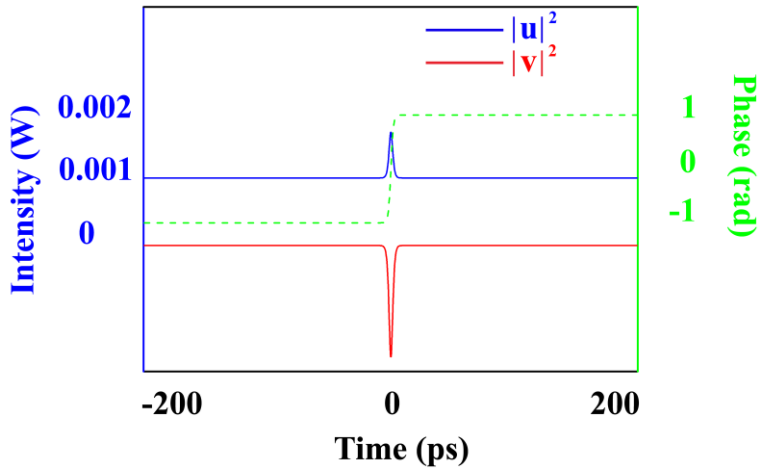

Fig. S13 Initially injected dark and antidark pulses with a slight walk-off between them. Bule solid line: Initial pulse shape for the antidark solitons. Red solid line: Initial pulse shape for the dark solitons. Green dashed line: initial phase jump for the antidark solitons.

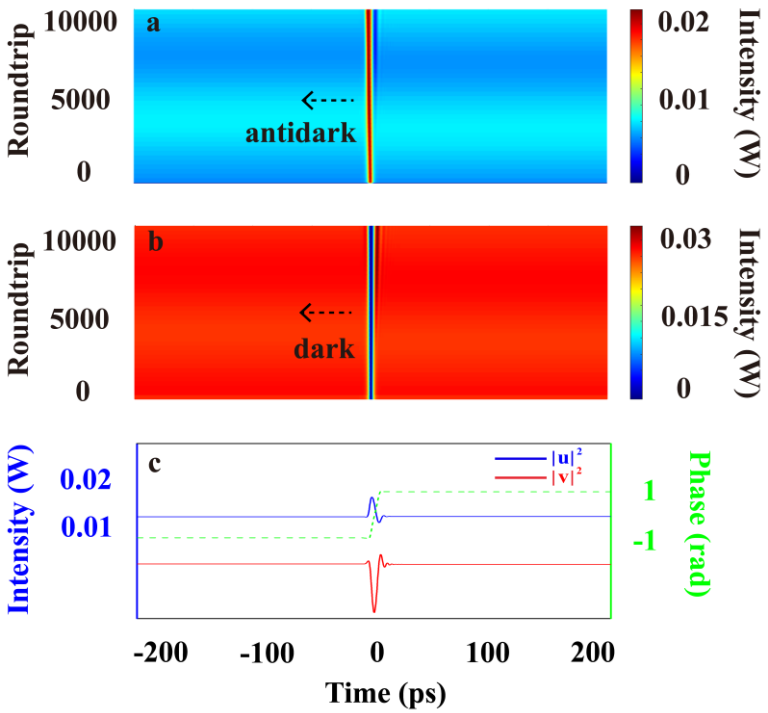

Fig. S14 Simulation results on formation of stable vector dark-antidark solitons. **a** Evolution of antidark solitons. **b** Evolution of dark solitons. **c** Red solid line: dark soliton at the last cavity round trip. Blue solid line: antidark soliton at the last cavity round trip. Green dashed line: phase jump properties for the antidark soliton at the last cavity roundtrip.

Our simulation is based on E. q. (3.1). We start the simulation with one pair of weak dark and antidark pulse. The dark pulse has the form of $\tanh(A \cdot t)$ and the antidark pulse has the form of $(0.001 + sech^2(A \cdot t))\exp(B \cdot i\tanh(t))$. To investigate the dispersion dependence of dark and antidark solitons, we deliberately set the dispersion coefficient of TOD to be $\beta_{3u,ave} = 0.1\ ps^3/km$ for the antidark solitons (which can be experimentally realized by tuning PC paddles until central wavelength emission close to the ZGVD point) and $\beta_{3v,ave} = 0.01\ ps^3/km$ for the dark solitons, as a result, vector dark-antidark solitons could be stably formed as shown in Fig. S14. Note that if we propagate the initial dark and antidark solitons with same TOD coefficient, i.e., $\beta_{3u,ave} = \beta_{3v,ave} = 0.01\ ps^3/km$, the antidark solitons will become unstable, similar to the case as shown in Fig. S12. This result again evidences that the antidark solitons could only be supported when TOD dominates GVD. Moreover, if we start the simulation with a small group velocity mismatch, i.e, $\delta = 0.0005\ ps/km$ along the orthogonal polarization axis by setting the beat length to be $L_B = 5\ km$, the dark and antidark solitons always trap with each other during their propagation in the cavity, they form a typical "1+1 soliton molecule" consisting of a dark soliton polarized along the vertical axis and an antidark soliton polarized along the horizontal axis, which agrees well with the experimental observation as shown in Figure 6 in the article. On the contrary, if we start the simulation with a large group velocity mismatch i.e, $\delta = 0.005\ ps/km$, this bound state between the dark and antidark soliton could be destroyed, as a result, the dark solitons are no longer captured by the antidark solitons polarized along the orthogonal polarization direction. Nonetheless, the one-component dark and antidark solitons could still be stably formed along the orthogonal polarization axis, propagating independently.

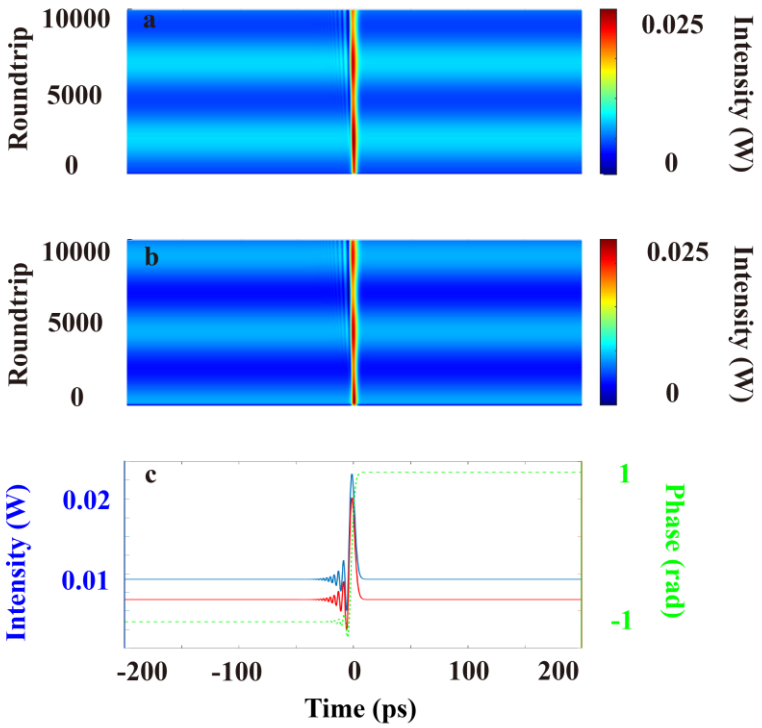

Fig. S15 Simulation results on influence of enhanced TOD. TOD coefficient increased to 0.2 ps^3/km; a-b) Antidark soliton evolution over 10000 cavity roundtrips along orthogonal polarization directions. c) Antidark soliton pattern at last cavity roundtrip.

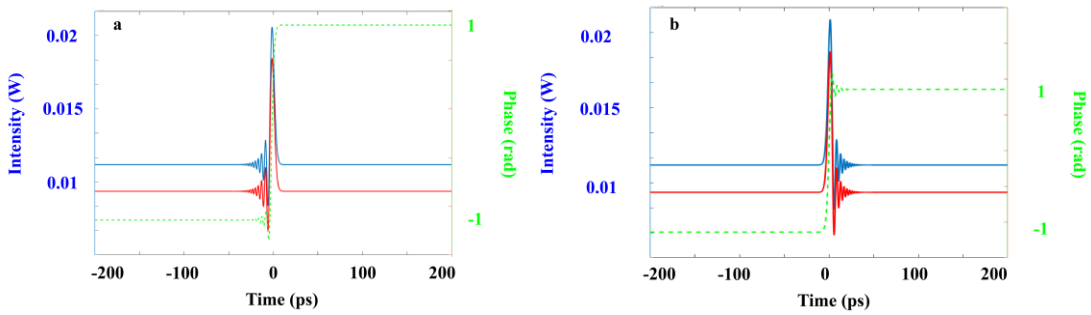

Fig. S16 Simulation results on influence of signs of TOD. a) TOD coefficient is -0.2 ps^3/km; b) TOD coefficient is 0.2 ps^3/km.

Numerically, we also study the formation of vector antidark solitons. Upon their formation, we investigate the influence of TOD on the antidark solitons. Our simulation model is based on E. q. (3.1). We start the simulation with one pair of weak antidark pulse. Each antidark pulse has the form of $(0.001 + sech^2(A \cdot t))\exp(B \cdot i\tanh(t))$. We first ensure that the dispersion satisfies the relation TOD > GVD to support the stable formation of antidark solitons, the simulation results are similar to those appeared in Fig. S14, and now a vector anti-dark soliton state is formed. Subsequently, in order to investigate the influence of TOD on the dynamics of

antidark solitons, we keep all the other simulation parameters unchanged except increasing TOD coefficient to 0.2 ps^3/km. The simulation results are shown in Fig. S15. It is clear that the enhancement of TOD will result in an oscillation tail on the antidark soliton envelop. Furthermore, we also investigate the influence of the sign of TOD on the antidark solitons. Interestingly, we found that the signs of TOD will result in oscillation tails appearing at opposite directions on the antidark soliton envelop as shown in Fig. S16. It is interesting to note that the appearance and the direction of these oscillation tails could strongly affect the internal interaction degrees of freedom of soliton molecules (SMs).

Initial Pulse Shape	Averaged cavity parameters	SMF	EDF	DCF
One pair of dark and antidark pulse in the form of $u = (0.001 + sech^2(A \cdot t))\exp(B \cdot i\tanh(t))$. $v = \tanh(A \cdot t)$ $A = 1$; $B = 0.1$;	*Net averaged cavity dispersion:* $\beta_{2v,ave} = \beta_{2u,ave} = 0.01\ ps^2/km$ $\beta_{3u,ave} = 0.1\ ps^3/km$ $\beta_{3v,ave} = 0.01\ ps^3/km$ *Net averaged cavity birefringence:* $\delta_{ave} = 0.0005\ ps/km$ γ =0.003 $(Wm)^{-1}$ Cavity loss: 10%	$\beta_{2u,SMF}$= -22.95 ps^2/km $\beta_{2v,SMF}$= -22.93 ps^2/km $L_B = 5\ km$ L=8.0 m	β_2= 63.4 ps^2/km g_0 = 90 km^{-1} Ω_g= 80 nm E_s=0.001 nJ $L_B = 5\ km$ L=3 m	β_2= 5.1 ps^2/km $L_B = 5\ km$ L= 0.2 m

Tab. S2. Parameters used for obtaining Fig. S14.

Section 6: Simulation results on formation of antidark soliton molecules

Fig. S17 shows the initial pulse shape we used for the simulations on two scalar antidark solitons. The details of the simulation parameters for Fig. S18 are described in Tab. S3.

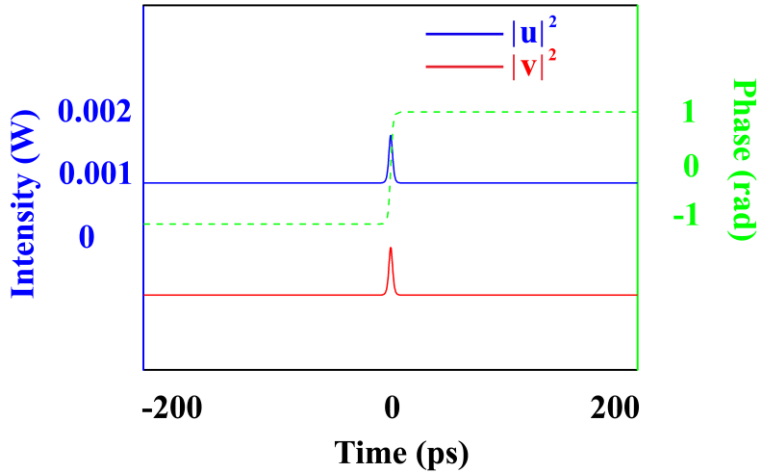

Fig. S17 Initially injected two antidark pulses with a slight walk-off between them. Bule solid line: Initial pulse shape for one of the antidark soliton. Red solid line: Initial pulse shape for another antidark soliton polarized along the same polarization. Green dashed line: initial phase jump for the antidark solitons.

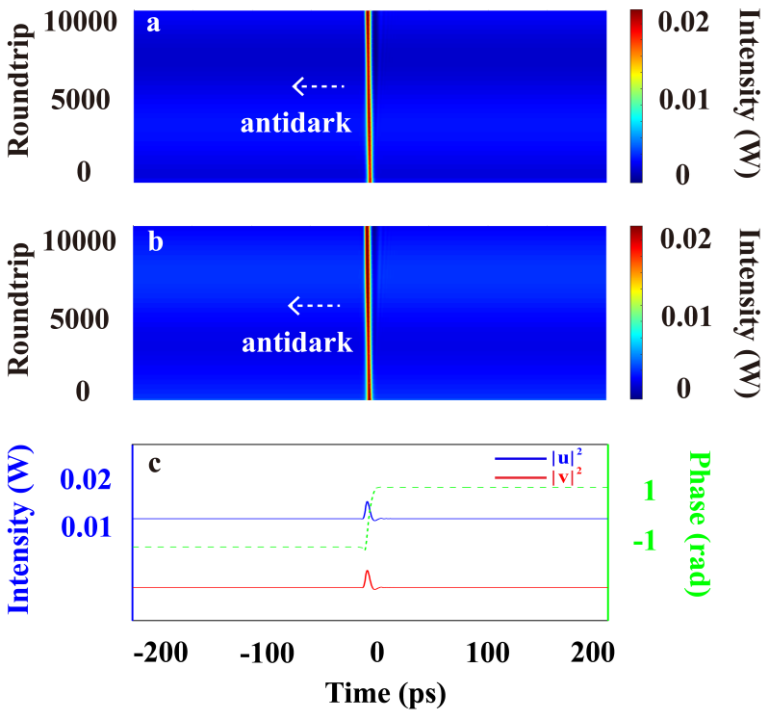

Fig. S18 Simulation results on one-component antidark soliton molecules. **a, b:** Evolution of the antidark solitons. **c** Red and blue solid lines: antidark solitons at the last cavity round trip. Green dashed line: phase jump properties for the antidark soliton at the last cavity roundtrip.

To numerically investigate the interactions between antidark solitons along the same polarization, we changed the XPM coefficient in the E. q. (3.1) to 2, thus, our simulation is conducted based on E. q. (3.3). We start the simulation with two antidark pulses, each in the form of $\left(0.001 + sech^2(A \cdot t)\right) \exp\left(B \cdot i\tanh(t)\right)$. First, to obtain the stable formation of antidark solitons, we must ensure that the TOD dominates GVD. To do this, we deliberately set the dispersion coefficient of TOD to $\beta_{3u,ave} = \beta_{3v,ave} = 0.1\, ps^3/km$, as a result of TOD dominance, two antidark solitons could be stably formed as shown in Fig. S18. Numerically, we have studied the interactions between the antidark solitons under two cases. First, we have checked that under a small group velocity mismatch, i.e, δ=0.0005 ps/km, a bound state of two antidark solitons are observed as shown in Fig. S18a-b. Specifically, they propagate towards left with the same group velocity, in the form of antidark soliton molecules which agree well with the results obtained in Figure 9 in the article. However, if the group velocity mismatch becomes large, eventually the attractive force between the neighboring antidark soliton is no longer strong enough to overcome the group velocity mismatch, a trapping state could be destroyed, consequently, the scalar antidark solitons will be independently formed and undergo collisions. Despite the antidark solitons undergo attractive interactions, numerically, we also verified that the interactions between scalar dark and antidark solitons are repulsive. Briefly, if we propagate an antidark and a dark pulse along the same polarization, irrespective of how weak the group velocity mismatch is, the dark and antidark solitons cannot form a bound state, which matches well with the theoretical predictions in [Eur. Phys. J. D **66**, 297 (2012)].

Initial Pulse Shape	Averaged cavity parameters	SMF	EDF	DCF
Two antidark pulses polarized along same polarization with each in the form of $u = (0.001 + sech^2(A \cdot t))\exp(B \cdot i\tanh(t))$. $v = (0.001 + sech^2(A \cdot t))\exp(B \cdot i\tanh(t))$ $A = 1$; $B = 0.1$;	*Net averaged cavity dispersion:* $\beta_{2v,ave} = \beta_{2u,ave} = 0.01\ ps^2/km$ $\beta_{3u,ave} = 0.1\ ps^3/km$ $\beta_{3v,ave} = 0.1\ ps^3/km$ *Net averaged cavity birefringence:* $\delta_{ave} = 0.0005\ ps/km$ γ =0.003 $(Wm)^{-1}$ Cavity loss: 10%	$\beta_{2u,SMF}$= -22.95 ps^2/km $\beta_{2v,SMF}$= -22.93 ps^2/km $L_B = 5\ km$ L=8.0 m	β_2= 63.4 ps^2/km g_0 = 90 km^{-1} Ω_g= 80 nm E_s=0.001 nJ $L_B = 5\ km$ L=3 m	β_2= 5.1 ps^2/km $L_B = 5\ km$ L= 0.2 m

Tab. S3. Parameters used for obtaining Fig. S18.